

Beware of CaBER: filament thinning rheometry doesn't give 'the' relaxation time of polymer solutions

A. Gaillard^{1†}, M. A. Herrada², A. Deblais¹, J. Eggers³ and D. Bonn¹

¹Van der Waals-Zeeman Institute, University of Amsterdam, Science Park 904, Amsterdam, Netherlands

²Depto. de Mecánica de Fluidos e Ingeniería Aeroespacial, Universidad de Sevilla, Sevilla E-41092, Spain

³School of Mathematics, University of Bristol, University Walk, Bristol BS8 1 TW, United Kingdom

(Received xx; revised xx; accepted xx)

Capillary Breakup Extensional Rheometry (CaBER) is commonly used to measure 'the' viscoelastic relaxation time τ of polymer solutions. We show experimentally that this method in fact only provides an apparent relaxation time that increases significantly when increasing the plate diameter and droplet volume. Similar results are obtained with a Dripping-onto-Substrate (DoS) method. This dependence on the flow history before the formation of the viscoelastic filament is in contradiction with polymer models such as Oldroyd-B that predict a filament thinning rate $1/3\tau$ which is a material property independent of geometrical factors. We show that this is not due to artefacts such as solvent evaporation or polymer degradation and that it cannot always be explained by the finite extensibility of polymer chains.

Key words: Viscoelasticity; Polymers; Capillary flows

1. Introduction

When polymers are added to a low-viscosity solvent such as water, the extensional rheology of the resulting solution is usually measured by indirect techniques where the (extensional) strain and strain rate are not controlled, unlike for high-viscosity polymer solutions or melts for which reliable extensional rheometers are available, e.g. Meissner's RME (Rheometric Melt Elongation rheometer) and FiSER (Filament Stretching Extensional Rheometer). Most indirect techniques for low-viscosity polymer solutions aim at forming a liquid filament undergoing capillary-driven thinning. Historically, this was first achieved by placing a drop of liquid between two horizontal plates which are then separated beyond the range of stable liquid bridges (Bazilevsky *et al.* 1997; Anna & McKinley 2001; Stelter *et al.* 2000), a technique now known as CaBER (Capillary Breakup Extensional Rheometry). Alternative techniques, also based on the Rayleigh-Plateau instability, were proposed to avoid inertio-capillary oscillations of the end-drops in the original CaBER step-strain (rapid) plate separation protocol which prohibits measurement of very short relaxation times (Rodd *et al.* 2004). The general idea is

† Email address for correspondence: antoine0gaillard@gmail.com

to generate a viscoelastic filament slowly, e.g. by separating the plates at a constant low velocity (Slow Retraction Method or SRM) (Campo-Deano & Clasen 2010), by dripping a droplet in air from a nozzle at a low flow rate (Tirtaatmadja *et al.* 2006) or, in a more recent technique, by slowly bringing a solid substrate in contact with a drop hanging steadily from a nozzle (Dripping-onto-Substrate or DoS) (Dinic *et al.* 2017).

In all these techniques, after an initial inertial and/or viscous regime, an elastic regime emerges where the elastic stresses arising from the stretching of polymer chains dominate and give rise to a cylindrical filament that thins exponentially in time for a wide range of dilute and semi-dilute polymer solutions. This is consistent with the Oldroyd-B model that predicts (Bazilevsky *et al.* 1990; Entov & Hinch 1997):

$$h = h_1 \exp\left(-\frac{t - t_1}{3\tau}\right) \quad (1.1)$$

where h is the minimum filament radius, τ the viscoelastic relaxation time of the polymer solution, t_1 the time marking the onset of the elastic regime, and $h_1 = h(t_1)$ the filament radius at that time. For a step-strain CaBER protocol, in which polymer molecules do not relax during the fast plate separation, the model predicts $h_1 = (Gh_i^4/2\gamma)^{1/3}$ where $G = \eta_p/\tau$ is the elastic modulus, η_p the polymer contribution to the shear-viscosity, γ the surface tension and h_i the radius of the initial liquid column (Clasen *et al.* 2006*a*). It is also generally accepted that for a polymer solution with a spectrum of relaxation times, the longest one rapidly dominates (Anna & McKinley 2001).

The general consensus is that geometrical parameters, in particular the size of the system, can only influence h_1 and not the thinning rate $|\dot{h}/h| = 1/3\tau$ of the filament since τ is a material property. In particular, Bazilevsky *et al.* (1997) and Miller *et al.* (2009) checked that the filament thinning rate was independent of the sample volume and of the plate separation speed and, in a step-strain plate separation protocol, on the final plate separation distance. This suggests that it is independent of the history of the polymer deformation prior to the elastic (exponential) regime. However, Rajesh *et al.* (2022) recently tested polymer solutions of different solvent viscosities with a dripping method and reported a larger thinning rate for a smaller nozzle radius.

In this communication, we investigate the role of the drop size on the thinning dynamics of CaBER filaments with a slow plate retraction protocol and show that CaBER does not measure the relaxation time properly; rather it yields an apparent relaxation time that depends on the way the viscoelastic filament is formed, and hence on the specific geometry used for the experiments.

2. Materials and methods

We use three different liquids: two solutions of poly(ethylene oxide) (PEO) of molecular weight $M_w = 4 \times 10^6$ g/mol, one in water with concentration 500 ppm, referred to as PEO_{aq}, and one in a more viscous solvent with concentration 25 ppm, referred to as PEO_{visc}, and a 1000 ppm solution of poly(acrylamide/sodium acrylate) (HPAM) [70:30] of molecular weight $M_w = 18 \times 10^6$ g/mol in water with 1 wt% NaCl to screen electrostatic interactions and make the chain flexible instead of semi-rigid. Both polymers were provided by Polysciences (ref. 04030-500 for PEO and 18522-100 for HPAM). For the PEO_{visc} solution, the solvent is an aqueous Newtonian 30 wt% 20,000 g/mol PEG solution. The different concentrations were chosen to ensure that all three liquids have comparable filament thinning rates. After slowly injecting the polymer powder to a vortex generated by a magnetic stirrer, solutions were homogenised using a mechanical stirrer at low rotation speed for about 16 hours.

Name	ρ (kg/m ³)	γ (mN/m)	η_s (mPa s)	c (ppm)	c/c^*	η_0 (mPa s)	η_p (mPa s)	n	$1/\dot{\gamma}_c$ (ms)	τ_m (ms)
PEO _{aq}	998	62.5	0.92	500	1.86	3.0	2.08	0.93	120	240
PEO _{visc}	1048	56.0	245	25	–	248	3.3	1	–	110
HPAM	998	72.0	0.92	1000	–	15	14	0.78	410	100

TABLE 1. Properties of the three polymer solutions. ρ is the density, γ the surface tension, η_s the solvent viscosity, c the polymer concentration, c^* the critical overlap concentration, η_0 , n and $\dot{\gamma}_c$ the Carreau fitting parameters of the shear viscosity, $\eta_p = \eta_0 - \eta_s$, and τ_m the maximum CaBER relaxation time measured for the largest plates.

The shear viscosity η of these solutions was measured at the temperature of filament thinning experiments with a MRC-302 rheometer from Anton Paar equipped with a cone plate geometry (diameter 50 mm, angle 1° and truncation gap 53 μm). The PEO_{visc} solution is a Boger fluid with a constant shear viscosity while the two others are shear-thinning and are well described by the Carreau law $\eta(\dot{\gamma}) = \eta_0(1 + (\dot{\gamma}/\dot{\gamma}_c)^2)^{(n-1)/2}$ where η_0 is the zero-shear viscosity, n is the shear-thinning exponent and $\dot{\gamma}_c$ is the shear rate marking the onset of shear thinning. These values, along with the solvent viscosity η_s , the density ρ and the surface tension γ measured with a pendent drop method, are reported in table 1. We also report the value of c/c^* for the PEO_{aq} solution for which viscosity measurements for different PEO concentrations gave an intrinsic viscosity $[\eta] = 2.87 \text{ m}^3/\text{kg}$ and hence a critical overlap concentration $c^* = 0.77/[\eta] = 0.268 \text{ kg/m}^3$.

In our home-made CaBER setup, a droplet of volume V is placed between two horizontal plates of radius R_0 and the top plate, which is controlled by a motor, is moved down until it is fully wetted by the liquid. As the top plate is moved up, a stable capillary bridge is formed, as shown in the left inset of figure 1(a). Beyond a certain critical value of the plate separation distance L , the bridge becomes unstable and collapses under the action of surface tension, transiently leading to the formation of a nearly cylindrical filament which is the signature of viscoelastic pinch-off, as shown in the right inset of figure 1(a). Instead of moving the top plate at a constant low velocity close to the bridge instability threshold, i.e. like in SRM (Campo-Deano & Clasen 2010), we move it by 10 μm steps, waiting about one second between each step (longer than the solution’s relaxation time) to allow polymers to relax back to equilibrium before the next step. We stop moving the top plate once capillary-driven thinning starts.

The process is recorded by a high-magnification objective mounted on a high-speed camera (Phantom TMX 7510) and images are analysed by a python code. A typical time-evolution of h is shown in figure 1(a). The purpose of this step-by-step plate separation protocol is to extract the value of the last stable bridge radius h_0 which, since steps are small, can be considered as the initial bridge radius at the onset of capillary thinning.

3. Results

Figure 1(b) compares the time-evolution of the minimum bridge / filament radius h for the PEO_{aq} solution tested with plate diameters $2R_0$ between 2 and 7 mm with a fixed non-dimensional droplet volume $V^* = V/R_0^3 \approx 2.4$. Although all filaments thin exponentially in time in the elastic regime, as suggested by the fairly straight curves, they thin faster for smaller plates. This is in apparent contradiction with the Oldroyd-B model which predicts a rate of exponential thinning $|\dot{h}/h| = 1/3\tau$ (see equation 1.1) which should be the same for all filaments, provided that the liquid doesn’t change so

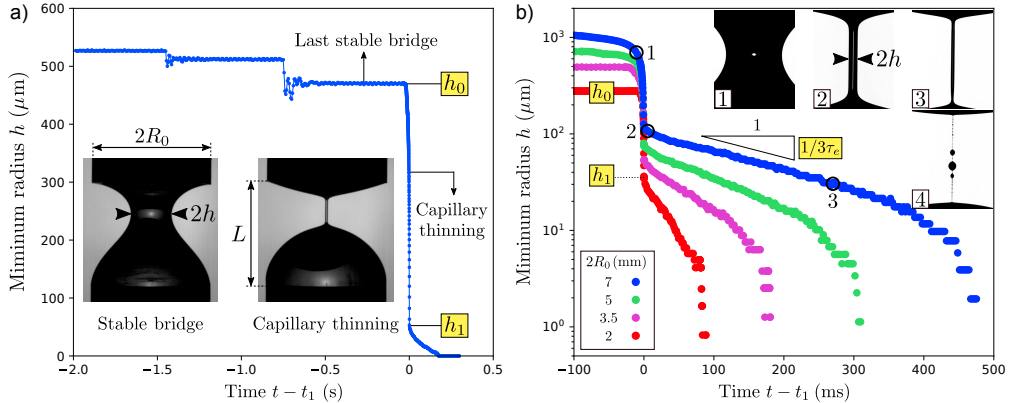


FIGURE 1. (a) Time evolution of the minimum bridge / filament radius h in the step-by-step plate separation protocol for the PEO_{aq} solution for plate diameters $2R_0 = 3.5$ mm and a droplet volume $V^* = V/R_0^3 \approx 2.4$. Inertio-capillary oscillations are visible after each step. Inset images correspond to a stable liquid bridge (left) and to a thinning filament of the same liquid with $2R_0 = 7$ mm and $V^* = 2.4$. (b) $h(t)$ in log-lin for the PEO_{aq} solution tested with plate diameters, $2R_0 = 2, 3.5, 5$ and 7 mm, with $V^* \approx 2.4$. Inset images correspond to three times labelled 1 to 3 indicated on the $h(t)$ curve plus a fourth later time where h is below our spatial resolution for $2R_0 = 7$ mm. The time reference t_1 marks the onset of the elastic regime.

that the (longest) relaxation time τ of the polymer solution is the same. As we present in Appendix A, similar results are found in DoS (Dripping-onto-Substrate) with filament thinning rates increasing with decreasing nozzle size.

To quantify these differences, we introduce an apparent (or effective) relaxation time τ_e such that $|\dot{h}/h| = 1/3\tau_e$ in the elastic regime. It is plotted in figure 2(a) as a function of the initial bridge radius h_0 for all polymer solutions, plate diameters and droplet volumes. We observe that τ_e increases with both R_0 and V^* and that all data points for a given solution collapse on a single curve when plotted against h_0 , which is itself an increasing function of both R_0 and V^* . This suggests that h_0 is in fact the only relevant geometrical parameter of the problem. This is in agreement with the accepted idea that polymer deformations during capillary thinning are only influenced by the local extensional flow in the bridge / filament of maximum extension rate $\dot{\epsilon} = -2\dot{h}/h$ at its thinnest point, where the dot means d/dt , while the top and bottom end droplets act as passive liquid reservoirs, their size not directly influencing the pinch-off dynamics.

The apparent relaxation time varies significantly, up to a factor 4 within the typical range of plate diameters used for CaBER experiments, see figure 2(a). However, the fairly linear increase of τ_e with h_0 in figure 2(a) cannot continue indefinitely. In order to observe the expected saturation of τ_e for larger values h_0 , we had to move to much larger plate diameters, up to $2R_0 = 25$ mm. For plate diameters $2R_0 \geq 10$ mm, the top end-drop doesn't cover the top plate fully because of gravity, as shown in the inset of figure 2(b). In fact, there is always a thin liquid film covering the top plate since we always clean the plates using plasma treatment, which makes the aluminium plates more hydrophilic and prevents dewetting. Note also that the top end-drop is not at the centre of the the top plate since the two plates are not perfectly parallel.

In spite of this lack of full coverage, we find that the critical minimum bridge radius h_0 marking the onset of the Rayleigh-Plateau instability increases with R_0 , allowing us to explore a wider range h_0 values, as shown in figure 2(b) where the apparent relaxation time τ_e seems to saturate to a maximum value τ_m , reported in table 1, at large h_0 . Since no clear plateau is observed, especially for the PEO_{aq} solution, the value of τ_m is only

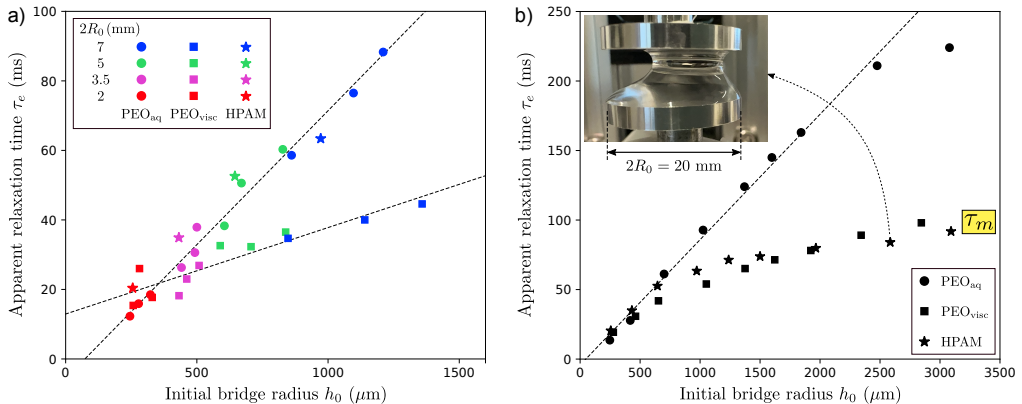


FIGURE 2. Apparent relaxation time τ_e against h_0 for all three solutions for plate diameters between 2 and 7 mm (a) and between 2 and 25 mm (b). In (a), data points of the same colour correspond to the same R_0 with different droplet volumes $V^* = V/R_0^3 \approx 1.3, 2.4$ and 3.2 . In (b), a single volume is used for each plate diameter ($V^* \approx 0.3$ for the smallest plates and 0.11 for the largest plates). The inset in (b) shows the shape of a stable liquid bridge for $2R_0 = 20$ mm.

an estimation. In figure 2(b), we only show one data point for each plate diameter, with V^* between 0.3 for the smallest plates and 0.11 for the largest plates.

Note that, the PEO solutions used in figures 2(b) are not the same as the ones used in figure 2(a) and have apparent relaxation times about 30% larger for $2R_0 = 7$ mm, while the shear viscosity was only up to 10 % larger, meaning that the shear rheology parameters in table 1 are representative of both solutions. These differences are due to slightly different preparation protocols, e.g. agitation times, for a given recipe.

4. Interpretations

The apparent disagreement between experiments and equation 1.1 implies that either the liquid changes, becoming less elastic for lower values of h_0 , or that the Oldroyd-B model, from which equation 1.1 is derived, misses some important features of polymer dynamics in extensional flows.

First of all, although the relaxation time measured in filament thinning is known to increase with polymer concentration (Tirtaatmadja *et al.* 2006; Clasen *et al.* 2006b), solvent evaporation can't explain the observed increase of the apparent relaxation time with increasing droplet size since the bulk polymer concentration would increase quicker for smaller droplets due to their larger surface to volume ratio, leading to larger concentrations for smaller droplets. Besides, all experiments are carried out at high relative humidity ($> 80\%$) and repeating an experiment several times over the course of 10 minutes doesn't lead to a monotonic increase or decrease of τ_e over time, beyond small variations of less than 5%. The latter observation also argues against polymer degradation as a possible explanation. Moreover, τ_e is observed to increase with h_0 for both PEO and HPAM solutions, even though HPAM is less fragile than PEO.

Therefore, if the liquid is in fact the same for each experiment, the Oldroyd-B model fails to describe the full polymer dynamics in the bridge / filament. In particular, differences in the history of polymer deformations for different drop sizes could lead to different "initial" states of polymers at the onset of the elastic regime, which could result in different filament thinning rates. We now discuss whether finite extensibility of polymer chains, as described by the FENE-P model, can account for such differences.

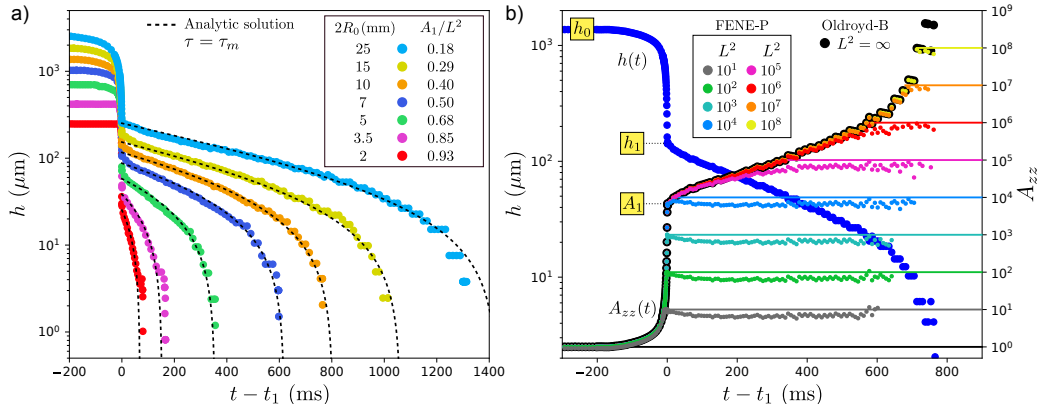


FIGURE 3. (a) $h(t)$ for the PEO_{aq} solution tested with different plate diameters. The elastic regime is fitted by equation 4.2 (see text) with $\tau = \tau_m$, using h_1 and A_1/L^2 as fitting parameters. (b) Time-evolution h from experiments and of A_{zz} calculated from equation 4.1 with $\dot{\epsilon} = -2\dot{h}/h$ using experimental values of h , with $\tau = \tau_m$ and various values L^2 for the PEO_{aq} solution tested with a plate diameter $2R_0 = 10$ mm, using $A_{zz} = 1$ at $h = h_0$ as the initial condition.

Following Wagner *et al.* (2015), for a uniaxial extensional flow, the polymeric part of the normal stress is $\sigma_{p,zz} = G(fA_{zz} - 1)$ in the flow direction z where G is the elastic modulus and A_{zz} is the normal part of the conformation tensor \mathbf{A} which follows

$$\dot{A}_{zz} - 2\dot{\epsilon}A_{zz} = -\frac{fA_{zz} - 1}{\tau}, \quad (4.1)$$

where $\dot{\epsilon}$ is the extension rate, τ the relaxation time and $f = (1 - \text{tr}(\mathbf{A})/L^2)^{-1}$ where L is the ratio of the fully unravelled chain size to its equilibrium size. In this model the stress diverges as A_{zz} approaches its limit value L^2 . In the elastic regime, we assume that polymers are far from equilibrium and that the axial stress dominates over the radial stress, i.e. $A_{zz} \gg 1 > A_{rr}$. Assuming negligible inertia and solvent viscosity, the force balance equation is $(2X - 1)\gamma/h = \sigma_{p,zz}$ with $X = 3/2$ in the Oldroyd-B limit (Eggers *et al.* 2020). Assuming a small correction due to finite extensibility, combining the force balance with equation 4.1 with $\dot{\epsilon} = -2\dot{h}/h$ leads to the ordinary differential equation $(3 + A_{zz}/L^2)\dot{A}_{zz} = A_{zz}/\tau$ which has an implicit solution

$$\frac{t - t_1}{\tau} = \frac{A_{zz} - A_1}{L^2} + 3 \ln \left(\frac{A_{zz}}{A_1} \right), \quad (4.2)$$

where $A_1 = A_{zz}(t_1)$ quantifies the amount of stretching of polymers in the z -direction at the onset of the elastic regime at time t_1 . In the Oldroyd-B limit $L^2 \rightarrow \infty$, we recover the expected exponential growth $A_{zz} = A_1 \exp((t - t_1)/3\tau)$. For a finite extensibility, the stress diverges and $h \rightarrow 0$ in finite time when A_{zz} saturates to L^2 , which occurs sooner as A_1/L^2 is closer to one. Consequently, as A_1 approaches L^2 , increasingly larger filament thinning rates will be observed. This is shown in figure 3(a) where the elastic regime of the PEO_{aq} solution, tested with different plate diameters, is compared with the predictions of equation 4.2 where we have chosen the maximum relaxation time τ_m measured at large h_0 as the relaxation time of the FENE-P model. We use the fact that, according to the force balance equation, the filament radius is $h/h_1 = f_1 A_1 / f A_{zz}$ where $f_1 = (1 - A_1/L^2)^{-1}$ and $h_1 = h(t_1)$. We use A_1/L^2 and h_1 as fitting parameters to obtain a good agreement between model and experiments. Most importantly, we have to impose that A_1/L^2 gets closer to one as h_0 decreases to capture the observed thinning rates, all larger than $1/3\tau_m$. For $2R_0 = 2$ mm for example, we need $A_1/L^2 = 0.93$, meaning that

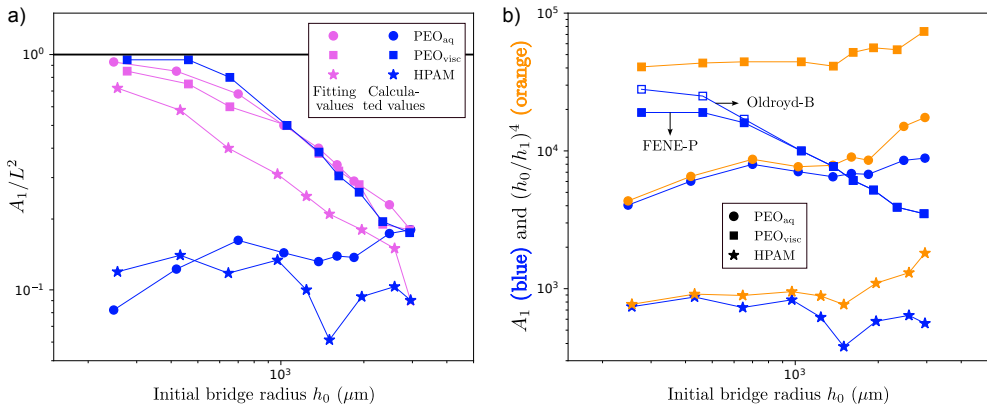


FIGURE 4. (a) Values of A_1/L^2 used as fitting parameters (light purple, see e.g. figure 3(a)), and values calculated from the FENE-P model (dark blue, see e.g. figure 3(b)) for $\tau = \tau_m$ and values of L^2 discussed in the text, against h_0 for all liquids and plate diameters. (b) Same values of A_1 calculated from the FENE-P model (dark blue), compared with $(h_0/h_1)^4$ (light orange). All values of A_1 calculated from FENE-P are the same as in Oldroyd-B except for the PEO_{visc} solution where Oldroyd-B values are shown with empty blue symbols.

polymers are almost fully extended at the onset of the elastic regime. Equally good fits can be obtained for the PEO_{visc} and HPAM solutions and the corresponding values of the fitting parameters A_1/L^2 are plotted against h_0 in figure 4(a) (light purple).

Although promising, this explanation is only valid if the FENE-P model indeed predicts that polymers are more stretched at the onset of the elastic regime as h_0 decreases. To test this, we use equation 4.1 to calculate $A_{zz}(t)$, using the experimental values of $h(t)$ for $\dot{\epsilon}(t) = -2\dot{h}/h$, although this expression is only valid at the thinnest bridge radius. In other words, we calculate the predictions of the model for the experimental history of extension rates. Importantly, we do *not* assume large polymer deformations ($A_{zz} \gg 1$), since polymers are at rest at the onset of capillary thinning, i.e. $A_{zz} = 1$ when $h = h_0$. We use $f = (1 - A_{zz}/L^2)^{-1}$ since when $f \neq 1$, axial stresses dominate over radial stresses. In order to circumvent the issue of calculating \dot{h} from experimental values of h , we introduce a function $y(t)$ such that $A_{zz} = y/h^4$, which gives $\dot{A}_{zz} + 4(\dot{h}/h)A_{zz} = \dot{y}/h^4$, so that equation 4.1 becomes $\tau\dot{y} = h^4 - y/(1 - y/(h^4L^2))$ which doesn't involve \dot{h} anymore. To solve this equation, we use a standard ODE solver, using spline interpolation to create a $t \rightarrow h(t)$ function based on experimental values of h . This equation can be integrated analytically in the Oldroyd-B limit, as shown by Bazilevsky *et al.* (2001).

The results are shown in figure 3(b) for the PEO_{aq} solution tested with a plate diameter $2R_0 = 10$ mm, with $\tau = \tau_m$ for the relaxation time of the FENE-P model, along with various values of L^2 , including the Oldroyd-B limit $L^2 \rightarrow +\infty$. As expected, values of A_{zz} calculated from FENE-P coincide with Oldroyd-B until it saturates when reaching L^2 . In particular, the value of A_1 becomes independent of L^2 when L^2 is sufficiently large and becomes indistinguishable from the values predicted by the Oldroyd-B model.

The values of A_1 calculated from the FENE-P model with $\tau = \tau_m$ are plotted in figure 4(a) against h_0 for all three solutions (dark blue) as A_1/L^2 where we chose $L^2 = 49000$, 20000 and 6200 for the PEO_{aq}, PEO_{visc} and HPAM solutions, respectively. For each liquid, the values of L^2 (a priori unknown) is chosen so that the calculated value of A_1/L^2 at the largest h_0 coincides exactly with the fitting value (light purple) used to fit the elastic regime with equation 4.2. We find that, while the fitting values of A_1 increase towards L^2 as h_0 decreases, the calculated values of A_1 only do so for the PEO_{visc}

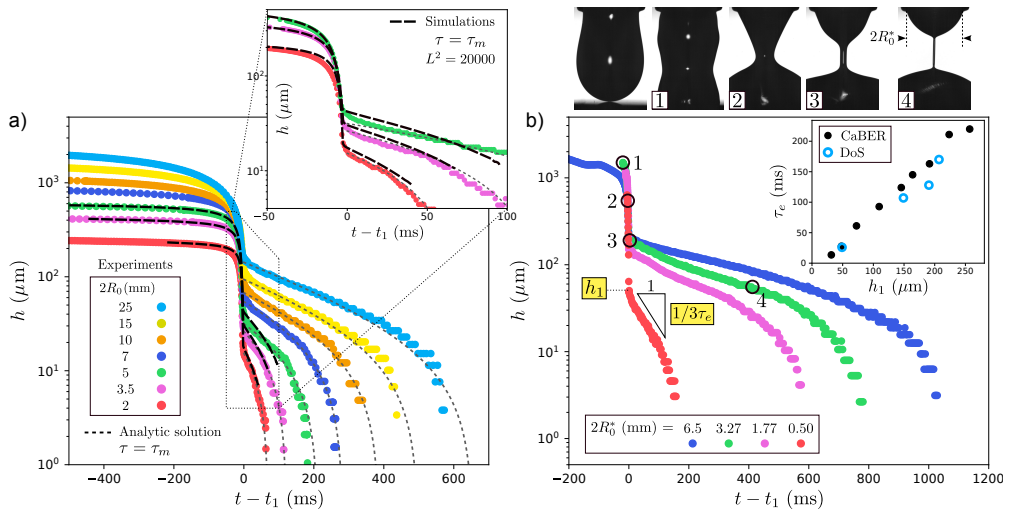


FIGURE 5. (a) $h(t)$ from experiments and simulations for the PEO_{visc} solution for different plate diameters. Simulations are performed for $2R_0 = 2, 3.5$ and 5 mm only, using the FENE-P model with $\tau = \tau_m$ and $L^2 = 20000$. The elastic regime is fitted by equation 4.2 where, like in figure 3(a), A_1/L^2 and h_1 are used as fitting parameters. (b) $h(t)$ from DoS experiments with different nozzle diameters for the PEO_{aq} solution. We report the values of the maximum diameter $2R_0^*$ of the top end-drop which is between the inner and outer nozzle diameter. Top images correspond to the steadily hanging drop (left) and to four times labelled 1 to 4 indicated on the $h(t)$ curve for $2R_0^* = 3.27$ mm. Inset: τ_e vs. h_1 from CaBER and DoS for the PEO_{aq} solution.

solution, for which a good agreement is found with the fitting values, and do not for the PEO_{aq} and HPAM solutions for which A_1 is fairly constant. For these last two, no other value of L^2 can lead to a better agreement since decreasing L^2 would just shift all calculated values towards the limit $A_1/L^2 = 1$.

In order to better understand this, we compare these calculated values of A_1 (dark blue) with their upper limit $(h_0/h_1)^4$ (light orange) in figure 4(b). This upper limit corresponds to a relaxation time τ so large that polymer relaxation (right hand side of equation 4.1) is always negligible in the Newtonian regime ($t < t_1$), a case where equation 4.1 can be integrated as $A_{zz}h^4 = h_0^4$. Differences in values of $(h_0/h_1)^4$ among the three polymer solutions are due to differences in h_1 which is an increasing function of η_p , as will be discussed in a separate paper. We find that A_1 is very close to the $(h_0/h_1)^4$ limit for the PEO_{aq} and HPAM solutions at low h_0 , with increasingly lower values as h_0 increases. This is consistent with the fact that the Deborah number $De = \tau_m/\tau_R$ decreases from 500 ($\gg 1$) to 5 as h_0 increases where $\tau_R = \sqrt{\rho h_0^3/\gamma}$ is the Rayleigh time scale relevant for the thinning dynamics of such low-viscosity liquids with Ohnesorge numbers $Oh = \eta_s/\sqrt{\rho\gamma h_0}$ up to $7 \times 10^{-3} \ll 1$. The greater difference between A_1 and $(h_0/h_1)^4$ for the PEO_{visc} solution in figure 4(b) is due to the slower thinning dynamics in the Newtonian regime, caused by a larger solvent viscosity with Ohnesorge numbers 270 times larger than for the two other solutions. As h_0 increases, the Newtonian thinning dynamics gets slower since the inertio- and visco-capillary time scales τ_R and $\tau_{\text{visc}} = \eta_s h_0/\gamma$ increase, which is the reason why A_1 decreases with h_0 for the PEO_{visc} solution.

The FENE-P model can hence only explain the increase of the apparent relaxation time τ_e with h_0 for the (dilute) PEO_{visc} solution, which has the highest solvent viscosity out of our three solutions. This is checked further by numerical simulations of the axisymmetric problem performed for fixed material properties η_s and η_p from shear rheology, $\tau = \tau_m$

and the value of $L^2 = 20000$ used in figure 4. The equations and numerical methods are details in Rubio *et al.* (2020). The results are shown in figure 5(a) for the three smallest plates and the corresponding experimental droplet volumes in terms of the time evolution of the minimum bridge / filament radius. Simulations are able to capture the Newtonian regime quite well and provide a reasonable agreement with experiments in the elastic regime. In particular, the filament thinning rate varies with the plate diameter, consistent with experiments, while the Oldroyd-B model would give a constant thinning rate $1/3\tau_m$. Simulations could not be continued far enough to compare with the full experimental time window. The figure also features the analytic solution 4.2 for the elastic regime where, like in figure 3(a), A_1/L^2 and h_1 are used as fitting parameters.

5. Conclusions and discussion

We have shown experimentally that the thinning rate of filaments of various polymer solutions is not just a material property but depends on the size of the system in both CaBER (with slow plate separation) and DoS experiments. Although all filaments are observed to thin exponentially, as predicted by the Oldroyd-B model (see equation 1.1), we show that the inferred apparent relaxation time τ_e measured in CaBER increases as the minimum bridge radius h_0 marking the onset of capillary thinning increases, which is a function of both the plate diameter and droplet volume, and seems to saturate at large h_0 . These observations hence suggest that CaBER relaxation times reported in the literature are not universal since testing a given polymer solution with different plate diameters and droplet volumes yields different results, at least for slow-plate-retraction CaBER protocols. We demonstrate that the variation of τ_e with h_0 is not caused by solvent evaporation or polymer degradation and can't be universally explained by finite extensibility effects described by the FENE-P model. These observations suggest that the single-mode Oldroyd-B and FENE-P models miss some important features of polymer dynamics in extensional flows.

A physical interpretation is still lacking and a better constitutive equation, capturing the deformation-history-dependent filament thinning rate, is needed. Models including a conformation-dependent drag accounting for hydrodynamic interactions between unravelling polymer chains in extensional flows could be the key.

Acknowledgements. We thank Louison Laruelle and Carmen van Poelgeest for preliminary experimental work.

Declaration of Interests. The authors report no conflict of interest.

Appendix A. Dripping-onto-substrate (DoS)

In DoS experiments, a horizontal substrate (here, a plasma-treated aluminium plate) is moved slowly upward until being in contact with a liquid droplet hanging steadily from a nozzle. As shown in the image sequence in figure 5(b), a fast spreading of the liquid on the plate leads to the pinch-off of the bridge connecting the substrate to the nozzle. This transiently leads to the formation of an exponentially thinning filament, as shown by the time-evolution of the minimum bridge / filament radius h in figure 5(b), where the PEO_{aq} solution is tested with four different nozzle diameters. As in CaBER experiments, the apparent relaxation time extracted from the filament thinning rate increases with the droplet size, here quantified by the nozzle diameter. This apparent relaxation time τ_e is plotted in the inset of figure 5(b) for both CaBER and DoS experiments against the

filament radius h_1 marking the onset of the elastic regime which, unlike h_0 in CaBER, is easily definable in both methods. The relatively good collapse of the data points on a single curve suggests a universal physical mechanism for the dependence of the apparent relaxation time on the size of the system, independent of the exact method used.

REFERENCES

- ANNA, S. L. & MCKINLEY, G. H. 2001 Elasto-capillary thinning and breakup of model elastic liquids. *Journal of Rheology* **45** (1), 115–138.
- BAZILEVSKY, AV, ENTOV, VM, LERNER, MM & ROZHKOV, AN 1997 Failure of polymer solution filaments. *Polymer Science Series ac/c of Vysokomolekuliarnye Soedineniia* **39**, 316–324.
- BAZILEVSKY, AV, ENTOV, VM & ROZHKOV, AN 1990 Liquid filament microrheometer and some of its applications. In *Third European Rheology Conference and Golden Jubilee Meeting of the British Society of Rheology*, pp. 41–43. Springer.
- BAZILEVSKY, AV, ENTOV, VM & ROZHKOV, AN 2001 Breakup of an oldroyd liquid bridge as a method for testing the rheological properties of polymer solutions. *Polymer Science Series AC/C of Vysokomolekuliarnye Soedineniia* **43** (7), 716–726.
- CAMPO-DEANO, L. & CLASEN, C. 2010 The slow retraction method (srn) for the determination of ultra-short relaxation times in capillary breakup extensional rheometry experiments. *Journal of Non-Newtonian Fluid Mechanics* **165** (23-24), 1688–1699.
- CLASEN, CHRISTIAN, EGGERS, JENS, FONTELOS, MARCO A, LI, JIE & MCKINLEY, GARETH H 2006a The beads-on-string structure of viscoelastic threads. *Journal of Fluid Mechanics* **556**, 283–308.
- CLASEN, C., PLOG, J. P., KULICKE, W.-M., OWENS, M., MACOSKO, C., SCRIVEN, L. E., VERANI, M. & MCKINLEY, G. H. 2006b How dilute are dilute solutions in extensional flows? *Journal of Rheology* **50** (6), 849–881.
- DINIC, JELENA, JIMENEZ, LEIDY NALLELY & SHARMA, VIVEK 2017 Pinch-off dynamics and dripping-onto-substrate (DoS) rheometry of complex fluids. *Lab on a Chip* **17** (3), 460–473.
- EGGERS, JENS, HERRADA, MIGUEL ANGEL & SNOEIJER, JH 2020 Self-similar breakup of polymeric threads as described by the oldroyd-b model. *Journal of fluid mechanics* **887**, A19.
- ENTOV, V. M. & HINCH, E. J. 1997 Effect of a spectrum of relaxation times on the capillary thinning of a filament of elastic liquid. *Journal of Non-Newtonian Fluid Mechanics* **72** (1), 31–53.
- MILLER, ERIK, CLASEN, CHRISTIAN & ROTHSTEIN, JONATHAN P 2009 The effect of step-stretch parameters on capillary breakup extensional rheology (caber) measurements. *Rheologica acta* **48**, 625–639.
- RAJESH, SREERAM, THIÉVENAZ, VIRGILE & SAURET, ALBAN 2022 Transition to the viscoelastic regime in the thinning of polymer solutions. *Soft Matter* **18** (16), 3147–3156.
- RODD, L. E., SCOTT, T. P., COOPER-WHITE, J. J. & MCKINLEY, G. H. 2004 Capillary break-up rheometry of low-viscosity elastic fluids .
- RUBIO, MANUEL, VEGA, EMILIO J, HERRADA, MIGUEL A, MONTANERO, JOSÉ M & GALINDO-ROSALES, FRANCISCO J 2020 Breakup of an electrified viscoelastic liquid bridge. *Physical Review E* **102** (3), 033103.
- STELTER, M, BRENN, GÜNTER, YARIN, AL, SINGH, RP & DURST, FRANZ 2000 Validation and application of a novel elongational device for polymer solutions. *Journal of Rheology* **44** (3), 595–616.
- TIRTAATMADJA, V., MCKINLEY, G. H. & COOPER-WHITE, J. J. 2006 Drop formation and breakup of low viscosity elastic fluids: Effects of molecular weight and concentration. *Physics of fluids* **18** (4), 043101.
- WAGNER, CAROLINE, BOUROUIBA, LYDIA & MCKINLEY, GARETH H 2015 An analytic solution for capillary thinning and breakup of FENE-P fluids. *Journal of Non-Newtonian Fluid Mechanics* **218**, 53–61.